Synthesis, characterization, and application of ruthenium-doped SrTiO₃ perovskite catalyst for microwave-assisted methane dry reforming

Lalit S. Gangurde[1], Guido S. J. Sturm[1], M. J. Valero-Romero[2], Reyes Mallada[3], Jesus Santamaria[3], Andrzej I. Stankiewicz[1], Georgios D. Stefanidis[1,4*]

[1]*Delft University of Technology, Process & Energy department, Intensified Reaction & Separation Systems, Leeghwaterstraat 39, 2628 CB, Delft, The Netherlands*

[2]*Catalysis Engineering, Department of Chemical Engineering, Delft University of technology, Van der Maasweg 9, 2629 HZ Delft, The Netherlands*

[3]*Institute of Nanoscience of Aragon and Department of Chemical Engineering and Environmental Technology C/ Mariano Esquillor, s/n, 50018, Zaragoza Spain.*

[4]*Katholieke Universiteit Leuven, Chemical Engineering Department, Celestijnenlaan 200F, 3001 Leuven, Belgium*

*Corresponding Author: Georgios D. Stefanidis

Email Address: georgios.stefanidis@kuleuven.be

Full postal address: Katholieke Universiteit Leuven, Chemical Engineering Department, Celestijnenlaan 200F, 3001, Leuven, Belgium

Abstract

A series of ruthenium-doped strontium titanate (SrTiO$_3$) perovskite catalysts were synthesized by conventional and microwave-assisted hydrothermal methods. The structure was analyzed by X-Ray diffraction (XRD) confirming the formation of the perovskite phase with some TiO$_2$ anatase phase in all the catalysts. Microwave irradiation decreases the temperature and time of synthesis from 220 °C for 24 h (conventional heating) to 180 °C for 1 h, without affecting the formation of perovskite. A 7 wt. % ruthenium-doped SrTiO$_3$ catalyst showed the best dielectric properties, and thus its catalytic activity was evaluated for the methane dry reforming reaction under microwave heating in a custom fixed-bed quartz reactor. Microwave power, CH$_4$:CO$_2$ vol. % feed ratio and gas hourly space velocity (GHSV) were varied in order to determine the best conditions for performing dry reforming with high reactants conversions and H$_2$/CO ratio. Stable maximum CH$_4$ and CO$_2$ conversions of ~99.5% and ~94%, respectively, at H$_2$/CO ~0.9 were possible to reach with the 7 wt. % ruthenium-doped SrTiO$_3$ catalyst exposed to maximum temperatures in the vicinity of 940 °C. A comparative theoretical scale-up study shows significant improvement in H$_2$ production capability in the case of the perovskite catalyst compared to carbon-based catalysts.

Keywords: Microwaves, methane dry reforming, perovskite catalysts, dielectric properties measurements

1. Introduction

Resource- and energy-efficient methane transformation to liquid fuels and chemicals is a research topic with societal, environmental and industrial relevance owing to the great variety of methane sources, including existing gas networks, small natural gas fields, shale gas, coal beds, agricultural biogas and deep-sea methane hydrates [1][2], the pressing issue of methane flaring in remote locations [3] and its significant contribution to the greenhouse effect [4][5][6].

A group of chemical routes to valorize methane includes its transformation into syngas (a mixture of CO and H_2) via steam reforming, dry reforming, partial oxidation and auto-thermal reforming. Among these processes, despite deactivation issues, dry reforming of methane (DRM) has 20% lower operating cost compared to the other mentioned processes [7]. DRM was first investigated as early as 1888 [8]. Fischer and Tropsch thoroughly explored DRM in 1928 [8]. This process reforms CH_4 and CO_2, both being greenhouse gases, into high purity syngas with negligible CO_2 content. The syngas from DRM can be used as direct feed for Fischer-Tropsch synthesis for selective synthesis of higher hydrocarbons [7].

The primary challenge for industrial implementation of DRM is the unavailability of commercial catalysts that can operate at the high temperatures (800 - 1000 ºC) required for CH_4 and CO_2 activation without catalyst deactivation issues due to carbon deposition [3]. The reported order of activity of noble and transition metals for DRM is Rh, Ru > Ir > Ni, Pt, Pd > Co > Fe, Cu [9]. Ruthenium has been reported to be the most active element combined with various supports such as Al_2O_3, La_2O_3, Y_2O_3, ZrO_2, TiO_2, MgO, SiO_2, carbon, and zeolites [9]. However, the high-temperature requirement of the highly endothermic DRM process leads to inevitable problems of

metal sintering and rapid catalyst deactivation. Therefore, catalytic materials with high thermal stability, activity and coking resistance are required [2].

Rapid and selective microwave heating has been reported to improve the performance of heterogeneous catalytic processes compared to conventional heating in one or more of the following terms (faster reaction rate, better product distribution, higher energy efficiency) [10–14]. One of the key factors determining the extent of these effects is the ability of the catalytic material to dissipate microwave energy (i.e., to become efficiently heated by microwaves). Therefore, it is important to measure the dielectric properties of the catalytic materials in the range of actual process conditions to verify the extent of their susceptibility to microwave heating.

Carbon materials have been used in the literature for microwave-assisted methane dry reforming as they are good MW receptors and catalytically active [15][16]. Dominguez et al. studied biogas to syngas by microwave-assisted dry reforming in the presence of char [17]. They reported that CH_4 conversion falls after some minutes due to blockage of the active centers by carbon deposits. Nevertheless, CH_4 conversion can be improved by the presence of CO_2, due to gasification of the carbon deposits. This effect was more noticeable in microwave heating than in conventional heating. It was also reported that constant removal of the carbon deposits was favored by the high K content in the char [17]. Most of the metal catalysts (e.g., Ni/Al_2O_3) that are active for DRM in conventional heating cannot be used directly for MW-assisted DRM because of their inability to reach the optimum reaction temperature due to their low dielectric properties. To address this issue, Fidalgo et al. mixed activated carbon with a metal-based catalyst to heat the latter up to the temperature required for MW-assisted DRM [18].

However, in our experiments, on microwave-assisted methane dry reforming over platinum on carbon catalyst, the amount of carbon catalyst decreased over a period of time (~ 270 min) and formed a carbon layer on the inner surface of the quartz wall of the reactor, thereby softening and eventually breaking the quartz tube wall [19]. Collectively, there is a room for the development of catalysts for MW-assisted methane dry reforming; such catalysts must have good microwave absorption ability, should be resistant to coke formation, should not get consumed during the reaction and produce high syngas yield.

Perovskite (ABO_3) materials have become attractive catalysts as they prevent agglomeration of metal ions by retaining their structure during high temperature reforming reactions [20]. They have potential applications in oxygen separators, solid oxide fuel cells and membrane reactors [21]. A typical perovskite is a structure with general composition type ABO_3. Perovskite oxides contain lanthanide elements at 'A' sites (for example, Ce, La, Pr) and a transition element at 'B' sites, such as Ni, Rh, Pt, etc. The significant advantages of the perovskite structure from the catalysis point of view are (1) its well-defined bulk structure with good oxygen storage capacity, (2) compositions at A and B cationic sites can be widely varied, (3) better thermal stability with valency control and (4) excellent redox properties [13]. Liu et al. studied several low-cost perovskite catalysts for auto-thermal reforming of n-dodecane and concluded that ruthenium-doped perovskite catalysts have superior reforming efficiency with good resistance to sulfur as compared to perovskite catalysts without ruthenium [22].

In this work, we have synthesized a series of Ru-doped $SrTiO_3$ perovskite catalysts by conventional and microwave-assisted hydrothermal methods. The catalysts have been characterized by X-ray diffraction (XRD), N_2 physisorption (BET surface area), inductively coupled plasma optical

emission spectrometry (ICP-OES) and high-angle annular dark-field scanning transmission electron microscopy (HAADF-STEM) coupled to energy dispersive X-ray (EDX) analysis. The dielectric properties have been measured in the temperature range 20 - 850 °C. The catalyst with the best dielectric properties was selected for application to DRM in a custom-built microwave reactor system. An experimental parametric study was carried out to investigate the role of microwave power, CO_2 concentration in the reaction mixture and gas hourly space velocity, as well as the catalyst stability. In this study, two-dimensional (2D) temperature monitoring was applied using an approach combining a thermal camera and thermocouples [19]. Finally, a comparison in terms of H_2 production between the synthesized perovskite catalyst and a carbon-based catalyst from the literature has been carried out for a theoretical scale-up scenario of the MW-assisted methane dry reforming process.

2. Experimental

2.1 Reagents and materials

Strontium nitrate ($Sr(NO_3)_2$, 99% ACS reagent), ruthenium(III) nitrosyl nitrate solution ($Ru(NO)(NO_3)_x(OH)_y$, x + y = 3), titanium dioxide (TiO_2, 99 %) and potassium hydroxide (KOH, 99%) were purchased from Sigma-Aldrich. All chemicals were used without any further purification.

2.2 Conventional hydrothermal (CHT) synthesis

A series of Ru-doped strontium titanate ($SrTiO_3$) perovskite catalysts were synthesized by conventional (C) and microwave-assisted (MW) hydrothermal methods. In the case of conventional hydrothermal method, stoichiometric amounts of $Sr(NO_3)_2$ (5.77, 5.70, 5.64 and 5.57 gm) and TiO_2

6

(2.18, 2.07, 1.96 and 1.85 gm), respectively, were separately dissolved in deionized water under stirring until complete solution. Subsequently, 0, 7.26, 14.36 and 21.29 ml of ruthenium (III) nitrosyl nitrate solution was added. The colloidal solution was stirred at room temperature for 10-20 min, and then a solution of 9M of KOH was added dropwise and kept for 6 h under stirring. The reaction mixture was then transferred to a teflon-lined stainless steel autoclave for hydrothermal treatment at 220 °C for 24 h [23]. After cooling down, the precipitates obtained were filtered off, washed with deionized water several times and dried at 80 °C for 6 h. The resulting solids were calcined at 800 ºC for 3 h to obtain the perovskite phase [24]. A heating rate of 5 ºC min^{-1} and static air conditions were applied to all the drying and calcination steps mentioned above. The samples prepared by conventional hydrothermal synthesis are denoted as yRu/SrTiO$_3$-C-zh, where y is the Ru content in *wt. %*, C stands for conventional heating, and z is the heating time in hours.

2.3 Microwave-assisted hydrothermal (MWHT) synthesis

In the case of microwave-assisted hydrothermal synthesis, the reaction mixture was prepared in a similar way to that mentioned in the conventional hydrothermal synthesis section. The only difference here is that the reaction mixture is placed in a teflon-lined autoclave inside a MILESTONE ETHOS Plus microwave cavity with automatic temperature control. The synthesis was performed at 220 °C for 6 h without stirring. Microwave synthesis while stirring the solution at a temperature of 180 °C for 1 h was also performed in order to reduce synthesis time and temperature. For 1 h MW synthesis with stirring, a MW setup (Mycrosynth plus model ACT38) with automatic temperature control (ATC-TO) was used. After the hydrothermal treatment, the reaction products were filtered off, washed with deionized water, dried and calcined under the conditions explained earlier in conventional hydrothermal synthesis. The samples prepared by microwave heating

are denoted as yRu/SrTiO₃-MW-zh, where y is the Ru content in *wt. %*, MW stands for microwave heating, and z is a heating time in hours.

2.4 Characterization methods

The crystalline phases of the powder catalysts were examined by X-ray powder diffraction (XRD) using a Bruker D8 Advance diffractometer. It is equipped with a Vantec position sensitive detector and a graphite monochromator. The measurements were performed at room temperature, using monochromatic Co Kα radiation (k = 0.179026 nm) in the 2θ region between 20 and 70°. The diffractometer was operating at 35 kV and 40 mA. The average crystallite size of perovskite in the catalysts was estimated from the Scherrer equation applied to the most intense diffraction (2θ = 37.77 °) using the shape factor K = 0.9. The phase compositions were semi-quantitatively estimated using Bruker Eva S-Q software. The reference intensity ratio (RIR) were taken from the PDF2 database (International Centre for Diffraction Data, 2004). A single reflection is used per phase; absorption correction is omitted, and the result is adjusted so that the sum of X_{phase} = 1. The reflections used were those with the highest intensities and without interference with other phases.

The dielectric properties of the prepared catalytic materials were measured by the DIMAS group at the Universitat Politecnica of Valencia, from 20 to 850 °C, in a dual mode cylindrical cavity by following the methodologies described elsewhere [25][26]. The catalytic samples were placed in a quartz tube, which was located inside the dual mode cylindrical cavity. The dielectric properties were measured while simultaneously heating the sample at 20 °C/min in N_2 atmosphere.

Textural properties of the materials were analyzed by N_2 adsorption-desorption at 77 K in a Tristar II 3020 Micromeritics sorptometer. Before each experiment, all the samples were outgassed at

8

200 °C for 16 h. From the N_2 adsorption/desorption isotherm, the specific surface area (S_{BET}) was determined from the BET equation [27]. The total pore volume (V_{total}) was determined from the adsorbed volume of N_2 at a relative pressure of 0.99.

Elemental analysis was performed using a PerkinElmer Optima instrument. Approximately 25 mg of each sample were digested in 4.5 ml 30% HCl + 1.5 ml 65% HNO_3 + 0.2 ml 40% HF using microwaves. The digestion time in the microwave oven was 30 min at maximum power. After digestion, the samples were diluted to 50 ml with MQ water and then analyzed by Inductively Coupled Plasma Optical Emission Spectrometry (ICP-OES) 5300DV.

High-resolution transmission electron micrographs were collected using (TEM/STEM) FEI Talos F200X, which operates at an accelerating voltage of 200 kV. To determine the specific distribution of elements present in the synthesized materials, energy dispersive X-ray (EDX) elemental maps were analyzed. Particle size distribution histograms were also obtained by counting around 100 particles from each sample.

2.5 Microwave-assisted dry reforming of methane (DRM)

Equation 1 represents the global DRM reaction that involves intermediate steps and side reactions. The intermediate steps (Equations 2 and 3) of methane cracking and carbon dioxide gasification both occur at high temperatures [17]. The most common side reactions (Equations 4 and 5) are the reverse water gas shift reaction (RWGS) (Equation 4), which occurs at temperatures lower than 820 °C and the Boudouard reaction (Equation 5), which occurs below 700 °C, contributing to the formation of carbon deposits [7].
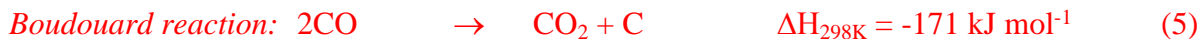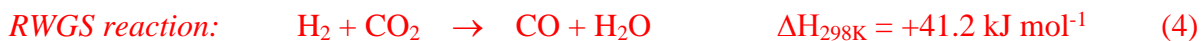
9

Global DRM Reaction: $CH_4 + CO_2 \rightarrow 2CO + 2H_2$ $\quad \Delta H_{298K} = +247 \text{ kJ.mol}^{-1}$ $\quad$ (1)

Intermediate Steps:

Methane Cracking: $\quad CH_4 \quad \rightarrow \quad C + 2H_2$ $\quad \Delta H_{298K} = +75.6 \text{ kJ.mol}^{-1}$ $\quad$ (2)

Carbon Gasification: $C + CO_2 \quad \rightarrow \quad 2CO$ $\quad \Delta H_{298K} = +172 \text{ kJ.mol}^{-1}$ $\quad$ (3)

(*Reverse Boudouard reaction*)

Side Reactions:

RWGS reaction: $\quad H_2 + CO_2 \quad \rightarrow \quad CO + H_2O$ $\quad \Delta H_{298K} = +41.2 \text{ kJ mol}^{-1}$ $\quad$ (4)

Boudouard reaction: $2CO \quad \rightarrow \quad CO_2 + C$ $\quad \Delta H_{298K} = -171 \text{ kJ mol}^{-1}$ $\quad$ (5)

The methane dry reforming experiments were performed in a specially developed microwave reactor system. Figure 1 shows the schematic diagram of the microwave reactor setup. For all the experiments, 1 g of $7Ru/SrTiO_3$-MW-1h (425-850 μm particle size), the catalyst with the highest loss tangent value among the tested series, was used to perform the DRM tests. The catalyst was loaded in a quartz tube (290 mm length × 8 mm i.d.) as shown in Figure 1. Two N-type thermocouples (-200 to +1250 °C) were placed at the top and bottom part of a catalyst bed to measure temperature at these positions. The quartz tube loaded with the catalyst was then inserted into the custom-designed microwave reactor, as shown in Figure 1.
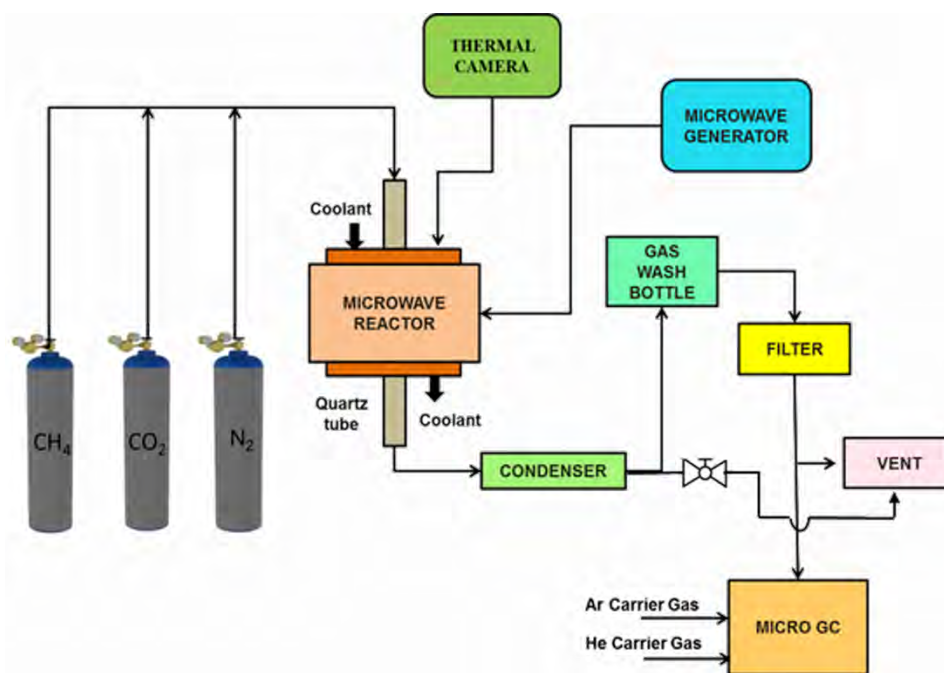
Figure 1: Schematic diagram of the microwave reactor setup [19]

A solid-state microwave generator (Miniflow 200 SS, 2.45 GHz) with a maximum power of 200 W was used to supply MW energy to the catalytic bed. The surface temperature of the catalytic bed in 2D fashion was monitored by a thermal camera, model FLIR A655sc (7.5 – 14 µm, -40 to 2000 °C). A thermostat was used to pump the coolant (ethylene glycol and water at 2:1 ratio) to the MW cavity, the condenser and the gas wash bottle. The MW cavity and condenser temperatures were always maintained at 8°C during the experiments to remove the heat from the cavity and the water from the outlet line of the reactor. After the condenser, a gas wash bottle filled with calcium oxide (CaO) was used to trap the remaining moisture present in the product gas line. The temperature of the gas wash bottle was maintained at -8°C in all the experiments. More details on the catalyst loading, the thermocouples positions to avoid their interaction with MW and on the operating procedure of the custom-designed microwave (MW) reactor are described in our recently published work [19].

The feed consisted of a mixture of CH_4 and CO_2. The total flow rate was varied from 50 to 225 ml min⁻¹ to achieve variable CH_4 and CO_2 conversion levels according to the residence time of the reactants. The product composition was analyzed by on-line gas chromatography (Varian CP4900 micro-GC), equipped with a TCD detector using two columns (20 m MS5A and 10 m PPU). The conversions of CH_4 and CO_2 were calculated by equations (6) and (7), respectively, considering the global DRM reaction (Equation 1) only.

$$CH_4 \text{ Conversion, } \% = 100 * \left[\frac{(H_2)Out}{2}\right] / \left[(CH_4)_{out} + \frac{(H_2)out}{2}\right] \quad (6)$$

$$CO_2 \text{ Conversion, } \% = 100 * \left[\frac{(CO)_{out}}{2}\right] / \left[(CO_2)_{out} + \frac{(CO)_{Out}}{2}\right] \quad (7)$$

Where $(CH_4)_{Out}$, $(H_2)_{out}$, $(CO_2)_{out}$ and $(CO)_{out}$ are methane, hydrogen, carbon dioxide and carbon monoxide concentrations in the effluent gas (% by volume). Approximately 100% of the MW power forwarded by the solid state generator to the sample is converted to heat; i.e., negligible reflected power is detected. MW power is mostly dissipated in the reactor itself, but, as reported by Cherbanski et al. [28], part of it may also be dissipated in the cavity walls, or in the hardware elements around the reactor.

The temperature of the catalytic material depends on its microwave heating ability under real process conditions. Therefore, methane dry reforming experiments were performed first with different MW powers to find out the optimum temperature response. After finding the optimum MW power, the influence of CO_2 concentration in the feed and of the total gas hourly space velocity (GHSV) on CH_4 conversion and overall reaction performance was studied. The total GHSV is defined by the ratio of total flow rate (cm^3h^{-1})/mass of catalyst (g), where the total flow rate is the

sum of the flow rates of CH_4 and CO_2. Finally, a stability test was performed at the optimum conditions of MW power, CH_4 to CO_2 ratio and GHSV for 3 h.

3. Results and discussion

3.1 Catalyst characterization

Figures 2a and 2b show the XRD patterns of Ru-doped $SrTiO_3$ perovskite catalysts synthesized by different methods, over different heating times, at different temperatures with or without stirring. Figure 2a shows a comparison of XRD patterns of all the $yRu/SrTiO_3$-C-24h conventionally synthesized catalysts with the $7Ru/SrTiO_3$-MW-1h catalyst. Figure 2b shows a comparison of all the $yRu/SrTiO_3$-MW-6h microwave synthesized catalysts with the $7Ru/SrTiO_3$-MW-1h catalyst. Bare $SrTiO_3$ (Fig. 2a) prepared by the conventional hydrothermal method exhibits diffractions at 37.8, 46.6, 54.4 and 68.2°, resulting from the presence of a perovskite cubic phase (PDF 73-0661). Ru-doped $SrTiO_3$ (3, 5 and 7 wt. % Ru) prepared by both conventional and microwave-assisted methods also exhibit perovskite reflections as the predominant phase (Figure 2a and 2b). However, those samples prepared under conventional heating also exhibit diffractions attributed to the anatase phase of TiO_2 as an impurity. These diffractions included intense peaks at 29.5 and 56.8° resulting from the presence of the anatase (101) and (200) crystal planes, respectively (PDF 78-2486).

Table 1 summarizes the semi-quantitative phase composition and the crystallite sizes of $SrTiO_3$ in the catalysts based on the Scherrer equation. The values of the specific surface area obtained by the BET method and the total pore volume derived from the N_2 adsorption data are also reported in Table 1. In general, the composition of $SrTiO_3$ is above 70 wt. % in all the catalysts; however, the presence of anatase increases for those samples prepared by microwave heating at the lowest

13

reaction time and temperature, 7Ru/SrTiO$_3$-MW-1h. Furthermore, the anatase composition decreases with increasing Ru loading and with increasing MW irradiation time and temperature; for example, it decreases from 26 wt.% for the bare SrTiO$_3$ (0Ru/SrTiO$_3$-C-24h) to 14 wt.% for the 7 wt.% Ru-doped SrTiO$_3$ (7Ru/SrTiO$_3$-C-24h) catalyst. The average crystallite sizes of bare SrTiO$_3$ and Ru-doped SrTiO$_3$ samples also showed differences, with smaller particles being formed in the samples with higher Ru loading. For instance, the average SrTiO$_3$ crystallite size decreases from 36.1 nm for 0Ru/SrTiO$_3$-MW-6h to 29.6 nm for 7Ru/SrTiO$_3$-MW-6h. These results suggest that the incorporation of Ru to SrTiO$_3$ could prevent particles sintering during the calcination step at 800 ºC. It is thus confirmed that the microwave-assisted preparation method can save energy and time due to the faster kinetics of crystallization [29].
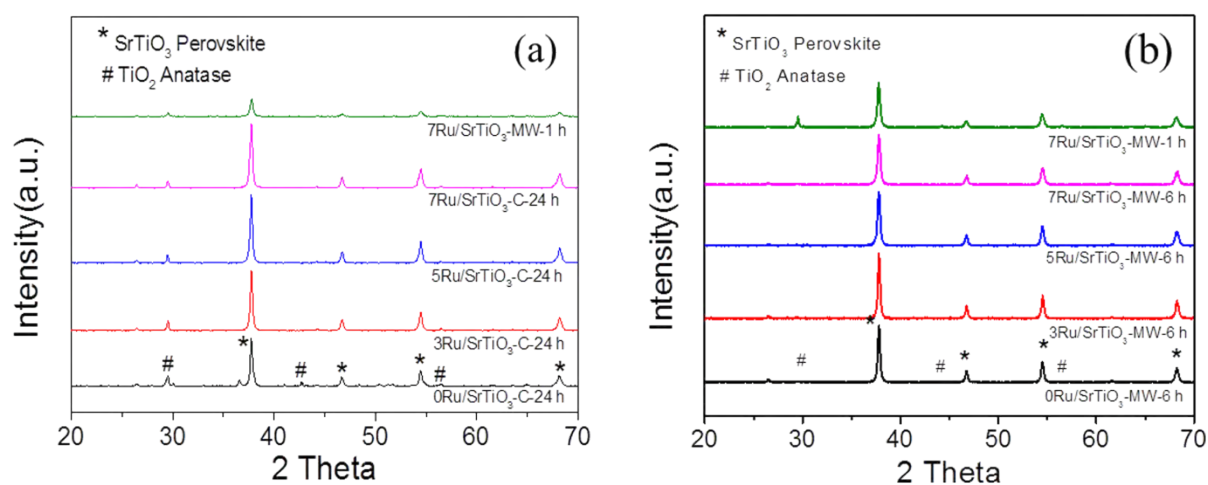

Figure 2. XRD patterns of **(a)** Ru-doped perovskite samples prepared by conventional HT synthesis for 24 h compared to MWHT for 1 h, and **(b)** Ru-doped perovskite samples prepared by MWHT synthesis for 6 h compared to MWHT 1 h.

Interestingly, the XRD of all the Ru-doped SrTiO$_3$ samples do not show any peak shifting or reflections corresponding to RuO$_2$ oxide formation, as reported before for Ru supported on SrTiO$_3$ [9]. This fact points out the high dispersion of ruthenium in SrTiO$_3$ prepared by hydrothermal

methods, both under conventional and microwave heating, despite the low BET surface areas and pore volume obtained.

The dielectric properties of the $yRu/SrTiO_3$-C-24h series samples have been measured and presented in Figure 3, while the specified weights and densities are presented in Table 2. The primary purpose of the dielectric properties measurements was to find a suitable catalyst for microwave heating and then use it for further characterization and the methane dry reforming reaction. Therefore, the dielectric properties of yRu-/$SrTiO_3$-MW-6h series and $7Ru/SrTiO_3$-MW-1h catalyst were not measured. The dielectric properties measurement procedure was explained in our recent work [19]. Specifically, heating up to 850 °C with a heating rate of 20 °C/min was carried out. In Figure 3a and 3b, the variation of the dielectric constant and loss factor with increasing temperature is presented for the $yRu/SrTiO_3$-C-24h series. For all the samples, the dielectric constant decreases with increasing temperature, whereas the loss factor increases with increasing temperature. Further, the dielectric constant and dielectric loss factor values increase with an increase in Ru content. From this comparison, it is clear that the $7Ru/SrTiO_3$-C-24h catalyst has the highest dielectric properties in the tested series.

Table 1: Physical and chemical properties of all synthesized Ru-doped $SrTiO_3$ catalysts.

	XRD			N_2 isotherm		ICP-OES
Catalyst	d_{SrTiO3}	S-Q_{TiO2} [a]	S-Q^a $_{SrTiO3}$	S_{BET}	V_{total}	Ru
	(nm)	(wt %)	(wt %)	(m^2/g)	(cm^3/g)	(wt%)
0Ru/SrTiO$_3$-**C-24h**	37.9	26.2	73.8	5	0.022	0
3Ru/SrTiO$_3$-**C-24h**	36.6	19.5	80.5	6	0.001	2.2
5Ru/SrTiO$_3$-**C-24h**	37.6	18.4	81.6	6	0.001	4.4
7Ru/SrTiO$_3$-**C-24h**	31.3	14.1	85.9	6	0.001	6.8
0Ru/SrTiO$_3$-**MW-6h**	36.1	1.9	98.1	8	0.032	0
3Ru/SrTiO$_3$-**MW-6h**	37.5	0.8	99.2	6	0.025	2.4
5Ru/SrTiO$_3$-**MW-6h**	30.0	1	99	6	0.020	4.8
7Ru/SrTiO$_3$-**MW-6h**	29.6	2.2	97.8	4	0.014	6.3
7Ru/SrTiO$_3$-**MW-1h**	29.8	22.2	77.8	8	0.026	7.2

[a] Semi-quantitative (S-Q) weight percentage of the phases obtained from XRD.

On the basis of the dielectric characterization presented, the 7 wt. % $Ru/SrTiO_3$-C-24h catalyst was selected for further microwave-assisted synthesis study. To study the role of reduction of synthesis temperature, time and stirring, microwave synthesis of this catalyst has been done at 220 °C for 6 h without stirring and at 180 °C for 1 h with stirring. As explained earlier, 1 h microwave hydrothermal synthesis with stirring has shown similar XRD peaks and confirmed the perovskite phase formation. The obtained catalyst is denoted as $7Ru/SrTiO_3$-MW-1h. Only the $7Ru/SrTiO_3$-C-24h and $7Ru/SrTiO_3$-MW-1h catalysts have been considered for further characterization and comparison purpose. Table 1 shows the elemental analysis results by ICP-OES. It indicates that higher concentration of the Ru element is present in the MW-synthesized catalyst ($7Ru/SrTiO_3$-MW-1h) as compared to the conventionally synthesized catalyst ($7Ru/SrTiO_3$-C-24h).

Table 2: Weights and densities of $yRu/SrTiO_3$-C-24h series used for dielectric properties measurements.

Sample	Catalyst Code	Weight(g)	Density(g/cm³)
1	$0Ru/SrTiO_3$-C-24h	1.498	1.2734
2	$3Ru/SrTiO_3$-C-24h	1.361	1.1673
3	$5Ru/SrTiO_3$-C-24h	1.271	1.0921
4	$7Ru/SrTiO_3$-C-24h	1.398	1.2120

To determine the dispersion of the different elements in the $7Ru/SrTiO_3$-C-24h and $7Ru/SrTiO_3$-MW-1h samples, high-angle annular dark-field scanning transmission electron microscopy (HAADF-STEM) images and energy dispersive X-ray (EDX) elemental maps have been produced. Figures 4 and 5 show the HAADF-STEM and EDX mapping of the $7Ru/SrTiO_3$-C-24h and $7Ru/SrTiO_3$-MW-1h catalysts, respectively. As shown in Figure 4, for $7Ru/SrTiO_3$-C-24h, the distribution of Ru, Sr, Ti and O elements is non-homogeneous indicating the random dispersion of the Ru element over the perovskite support. On the other hand, the $7Ru/SrTiO_3$-MW-1h catalyst (Figure 5) shows a homogeneous dispersion of all the elements, suggesting that stirring the mixture

during the hydrothermal synthesis is crucial for proper dispersion of Ru. Therefore, not only MW irradiation improved the catalyst preparation in terms of time and energy, but also stirring enables good dispersion of the elements.
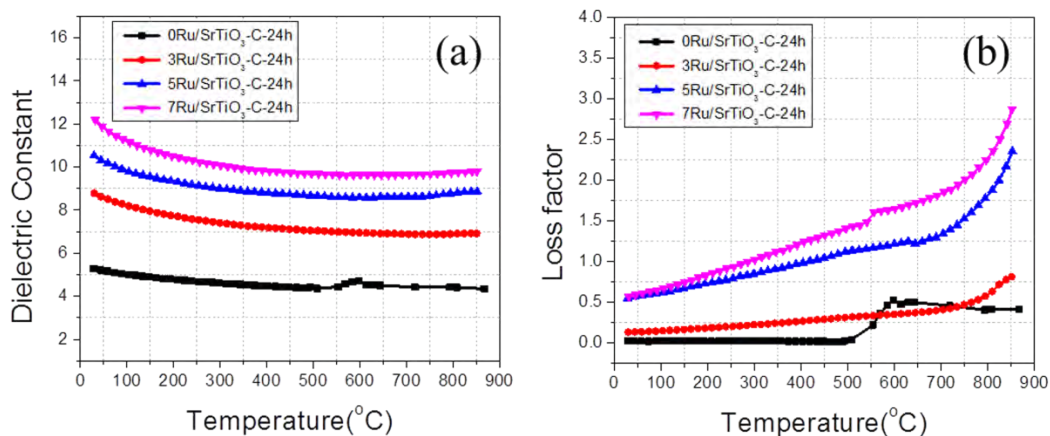

Figure 3: (a) Dielectric constant versus temperature and **(b)** loss factor versus temperature for the yRu/SrTiO₃-C-24h catalyst series.
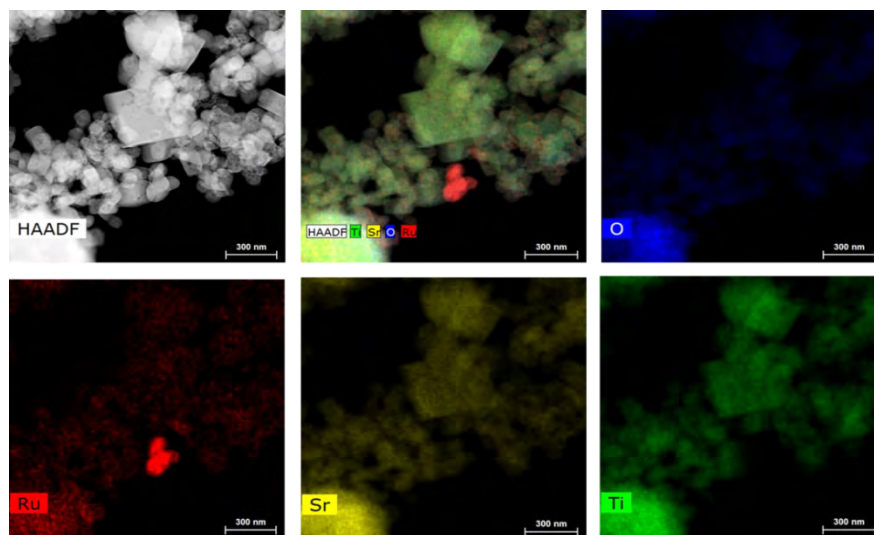

Figure 4. HAADF-STEM image and EDX elemental maps of O, Ru, Sr and Ti for the 7Ru/SrTiO₃-C-24h catalyst.

Finally, the morphology of both catalysts prepared under conventional(C) and MW hydrothermal synthesis methods are compared. Figure 6 shows TEM images and particle size distributions of 7Ru/SrTiO$_3$-C-24h (a, c) and 7Ru/SrTiO$_3$-MW-1h (b, d). The 7Ru/SrTiO$_3$-C-24h catalyst, prepared under conventional heating, shows a wider range of particles sizes, from around 120 nm to around 300-500 nm particles (in lower proportion). 7Ru/SrTiO$_3$-MW-1h shows a more homogeneous particle size distribution of around 100 nm. The production of bigger particles shown in Figure 6(a, c) might be due to the longer hydrothermal reaction time and higher temperatures than in the case of MW heating, where the shorter reaction time and lower temperature result in more homogeneous particle sizes due to the stirring effect. Nonhomogeneous particles sizes and bigger particles could favour nonhomogeneous MW field distribution during the reaction. In the case of 7Ru/SrTiO$_3$-MW-1h, the homogeneous distribution of Ru and the homogeneous particle size with better dielectric properties could contribute to better heat transfer in the catalyst bed under MW irradiation. Therefore, only the 7Ru/SrTiO$_3$-MW-1h catalyst has been selected for the microwave-assisted methane dry reforming reaction.
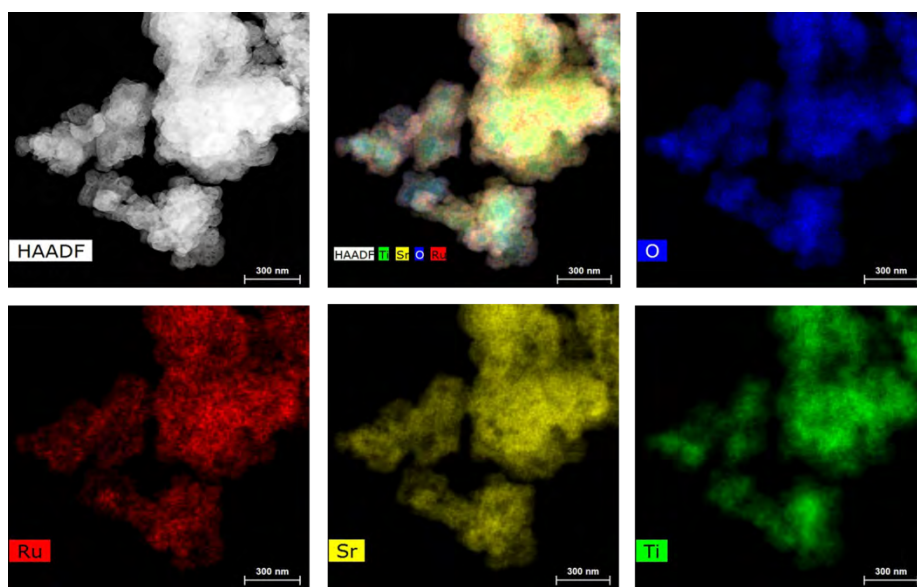

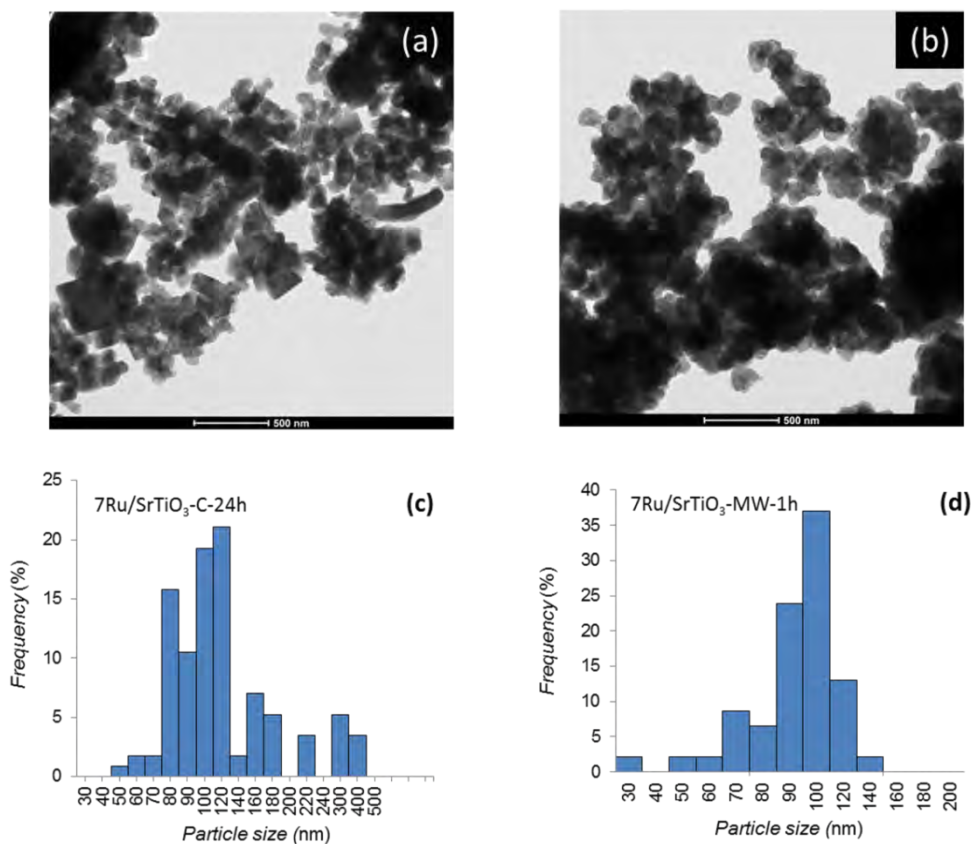**Figure 5.** HAADF-STEM image and EDX elemental maps of O, Ru, Sr and Ti for the 7Ru/SrTiO$_3$-MW-1h catalyst.

18

Figure 6. TEM images and particle size distributions of 7Ru/SrTiO$_3$-C-24h (a, c) and 7Ru/SrTiO$_3$-MW-1h (b, d)

3.2 Catalytic reactor performance

3.2.1 Reactor thermal response at varying MW input

A parametric study with variable MW power input was performed to a) obtain understanding of the thermal response of the catalytic bed as function of MW power at real reaction conditions and avoid any kind of quartz reactor damage due to overheating [30,31]; b) find the power settings at which reactor temperature is high enough to maximize reactants conversion. Figure 7 shows (a) CH$_4$ and CO$_2$ conversion and (b) H$_2$/CO ratio and temperature of the catalytic bed under real reaction

19

conditions of the methane dry reforming process as function of MW power in the range 30 to 90 W. Each MW power was tested for 20 min and then increased by 10 W up to 90 W.

Figure 7a shows that CH_4 and CO_2 conversions expectedly increase with increasing MW power and CO_2 conversion is always lower than that of CH_4. Figure 7b shows that the H_2/CO ratio increased from 0.60 to 0.89 and remained ~0.86 at ~90 W where the top bed temperature observed was 1067.6 °C (Figure 7b). Figure 7b shows that the temperature at the top of the catalytic bed increased with increasing MW power from 414.9 °C at 30 W to 1067.6 °C at 90 W. As temperature distribution is not homogeneous in the catalytic bed, the reaction will not be occurring homogeneously over the catalytic bed. Therefore, it was found from this study that in order to reach a temperature of ~1000 °C or get maximum reactants conversions, a minimum power of 90 W is required.
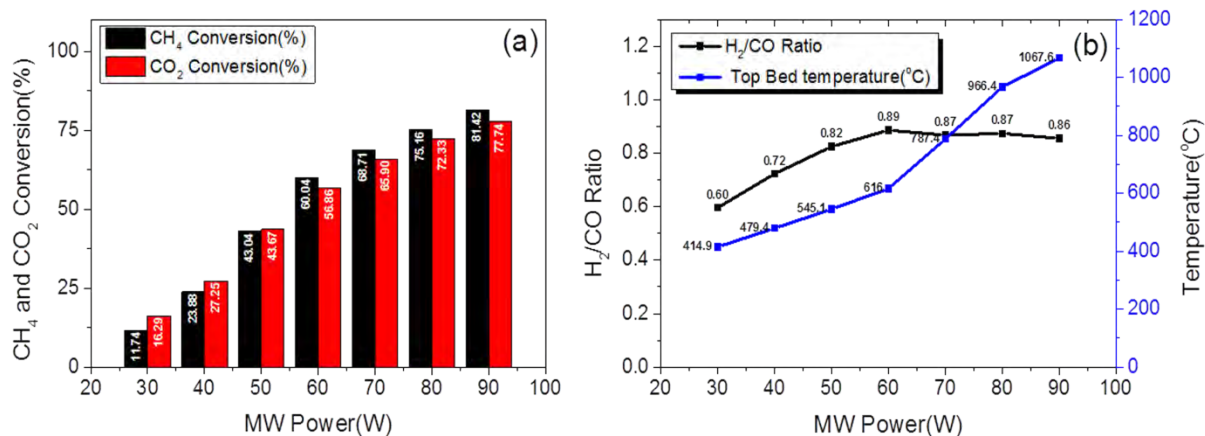

Figure 7. Effect of microwave power on **(a)** CH_4 and CO_2 conversion, **(b)** H_2/CO ratio and temperature at the top of the bed for the $7Ru/SrTiO_3$-MW-1h catalyst. (Reaction conditions: CH_4:CO_2 vol. % feed ratio 50:50, GHSV = 3000 $cm^3g^{-1}h^{-1}$)

3.3.2. Effect of CO_2 concentration in the feed

Figure 8 shows the effect of CO_2 concentration in the gas feed on the reactants conversion and the temperature at the top of the reactor filled with the $7Ru/SrTiO_3$-MW-1h catalyst. The total flow of reactant gas mixture was 50 ml/min with a constant MW power of 90 W. The CO_2 concentrations (vol. %) applied were 45, 50, 55 and 60 % in total flow. Each flow has been applied for 30 min. It has been reported in the literature that CH_4 conversion decreases after long reaction time due to carbon deposition [32][33]. Carbon deposition or coke formation during the DRM process is the major reason for deactivation of the catalytic sites in conventional heating.
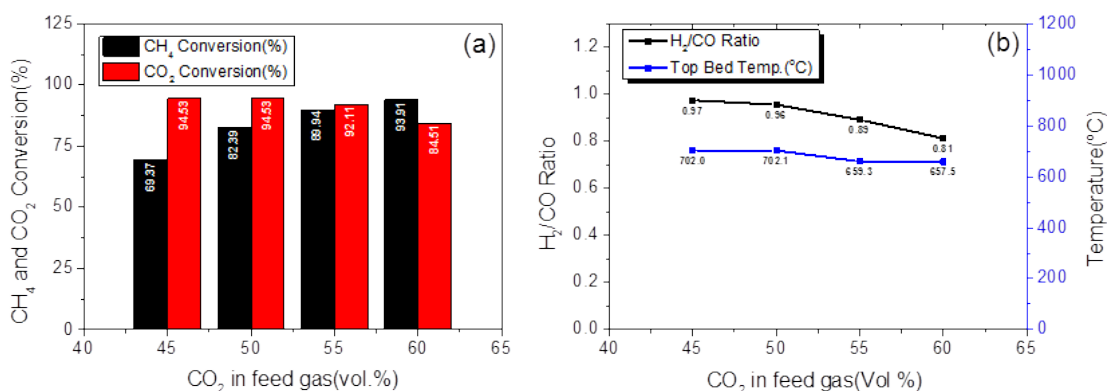

Figure 8: Effect of CO_2 concentration (vol. %) on **(a)** CH_4 and CO_2 conversion,

(b) H_2/CO ratio and temperature at the top of the bed for the $7Ru/SrTiO_3$-MW-1h catalyst.

(Reaction Conditions: GHSV = 3000 $cm^3g^{-1}h^{-1}$, MW power: 90 W)

Dry reforming of methane ($CH_4 + CO_2 \leftrightarrow 2H_2 + 2CO$) involves combination of two reactions namely, catalytic methane decomposition ($CH_4 \rightarrow C + 2H_2$) and CO_2 gasification ($C + CO_2 \leftrightarrow 2CO$) [17]. It has been reported that under microwave heating, increasing concentration of CO_2 in the reaction mixture results in increased gasification rate of the deposited carbon and thereby faster regeneration of the active sites and increase in CH_4 conversion [17][16][34]. This is in agreement with our experimental results too. Figure 8a and 8b show that as CO_2 concentration (vol. %)

21

increases from 45 to 60% at constant MW power input of 90 W, CH_4 conversion increases from 69.37 to 93.91%, while H_2/CO ratio decreases from 0.97 to 0.81 and temperature at the top of the bed decreases from 702 to 657.5 °C.

3.3.3. Gas Hourly Space Velocity (GHSV) study

Figure 9 shows the effect of total GHSV on (a) CH_4 and CO_2 conversion, (b) H_2/CO ratio and the temperature at the top of the catalytic bed for the 7Ru/SrTiO$_3$-MW-1h catalyst. Increase in the total flow requires higher MW power input to maintain a targeted top bed temperature and high conversions. The GHSV and corresponding powers applied are reported in Table 3. As we observed that a temperature of ~700 °C at the top of the catalytic bed was the optimum one to get maximum conversions, we tried to maintain that temperature, and therefore power has been increased or decreased as per the behavior of the catalytic material to maintain the targeted top catalytic bed temperature.

Table 3: GHSV study with CH_4:CO_2 vol. % feed ratio 45:55

and corresponding MW powers applied.

Test. No.	Total flow (ml/min)	MW Power used (W)	Total VHSV ($cm^3g^{-1}h^{-1}$)
1	50	90	3000
2	75	105	4500
3	100	110	6000
4	125	120	7500
5	150	135	9000
6	175	150	10500
7	200	165	12000
8	225	160	13500

Each flow has been applied for 30 min. Figure 9a shows that CH_4 and CO_2 conversions were high up to a total GHSV of 10500 $cm^3g^{-1}h^{-1}$, but at 12000 $cm^3g^{-1}h^{-1}$, the conversions dropped at ~61.78% and ~63.57% for CH_4 and CO_2, respectively. Lower conversions accompanied by a simultaneous

increase in temperature, as the reaction is endothermic, were observed for the last two (highest) GHSV tests, which indicates that the reactants residence time is not sufficient to reach the high conversions (>90%) obtained at GHSVs <10500 $cm^3g^{-1}h^{-1}$. Finally, Figure 9b shows that increase in the total GHSV does not have much influence on the H_2/CO ratio, which remained in the range from 0.85 to 0.9.
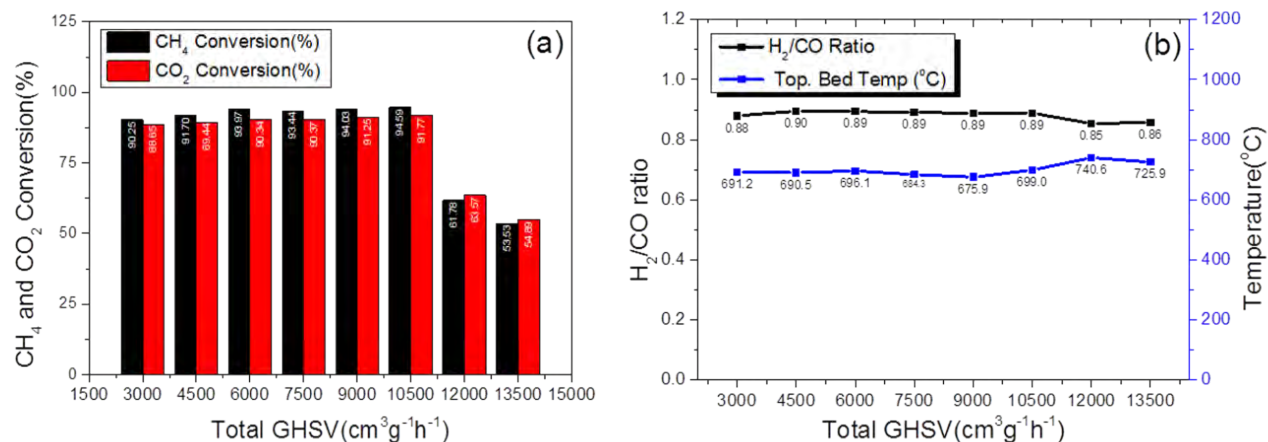

Figure 9. Effect of total GHSV on **(a)** CH_4 and CO_2 conversion, **(b)** H_2/CO ratio and temperature at the top of the catalytic bed for the $7Ru/SrTiO_3$-MW-1h catalyst. (Reaction conditions: $CH_4:CO_2$ vol. % feed ratio 45:55; corresponding MW powers applied are specified in Table 3)

3.3.4. Catalyst stability study

Figure 10 shows time-on-stream (TOS) evolution of (a) CH_4 and CO_2 conversions, (b) top and bottom thermocouple temperatures of the catalyst bed, (c) MW power and the H_2/CO ratio and (d) % MW energy utilization efficiency during methane dry reforming on the $7Ru/SrTiO_3$-MW-1h catalyst. The TOS study has been performed at GHSV = 9000 $cm^3g^{-1}h^{-1}$, MW Power 150 W and $CH_4:CO_2$ vol.% feed ratio 45:55. It was concluded from the GHSV study presented in Table 3 that maximum conversion at 9000 $cm^3g^{-1}h^{-1}$ GHSV requires MW power of 135 W. Therefore, the reaction was initially started with 135 W, and after some time, the MW power was increased to 150

W, corresponding to a top thermocouple temperature of ~500°C, as shown in Figure 10b, to maintain maximum conversions of reactants.

Figure 10a and 10c show that the CH_4 and CO_2 conversions depend on the MW power applied. Figure 10d shows that 100% microwave energy utilization efficiency was achieved during 180 min of TOS due to the excellent MW absorption ability of the catalyst and the reactor configuration that allows for concentration of the MW field on the catalyst itself. Both reactants conversions increased with increase in the MW power and reached maximum values at 150 W. Figure 10a shows that CO_2 conversion was lower than CH_4, due to the excess of CO_2 in the feed (CH_4:CO_2 vol. % feed ratio 45:55) during the stability test. As a result, the H_2/CO product ratio was lower than one (~ 0.9).

Zhang et al. studied CO_2 reforming of methane on Pt-based catalysts using microwave heating [35]. They reported that the higher reactants conversions under microwave heating, compared to conventional heating, is attributed to the formation of hot spots, which are at a higher temperature than the average catalytic bed temperature [35]. Therefore, to verify such temperature gradients during the stability test, the temperature distribution in the catalytic bed was monitored by a thermal camera in a 2D fashion. The following section (3.3.5) provides a more detailed explanation of hotspots generation and the induced spatial temperature deferences.

In addition to MW hotspot effect, placement of Ru in the perovskite structure also plays an essential role as it prevents metal sintering at high temperatures (~800°C)[9]. The improved catalytic behavior of the Ru-containing catalysts could be related to the participation of bulk oxygen during the reaction that enhances reactants adsorption [20]. Further, the constant removal of carbon deposits under MW heating promotes catalyst regeneration. Therefore, the stable high conversions

observed at relatively low top bed temperature ~500 °C are due to the presence of hot spots in the catalyst bed, the stability of perovskite structure that prevents sintering, the good redox properties of the perovskite catalyst, and, possibly, the regeneration of the active catalytic sites due to continuous coke removal through CO_2 gasification under MW heating [16].
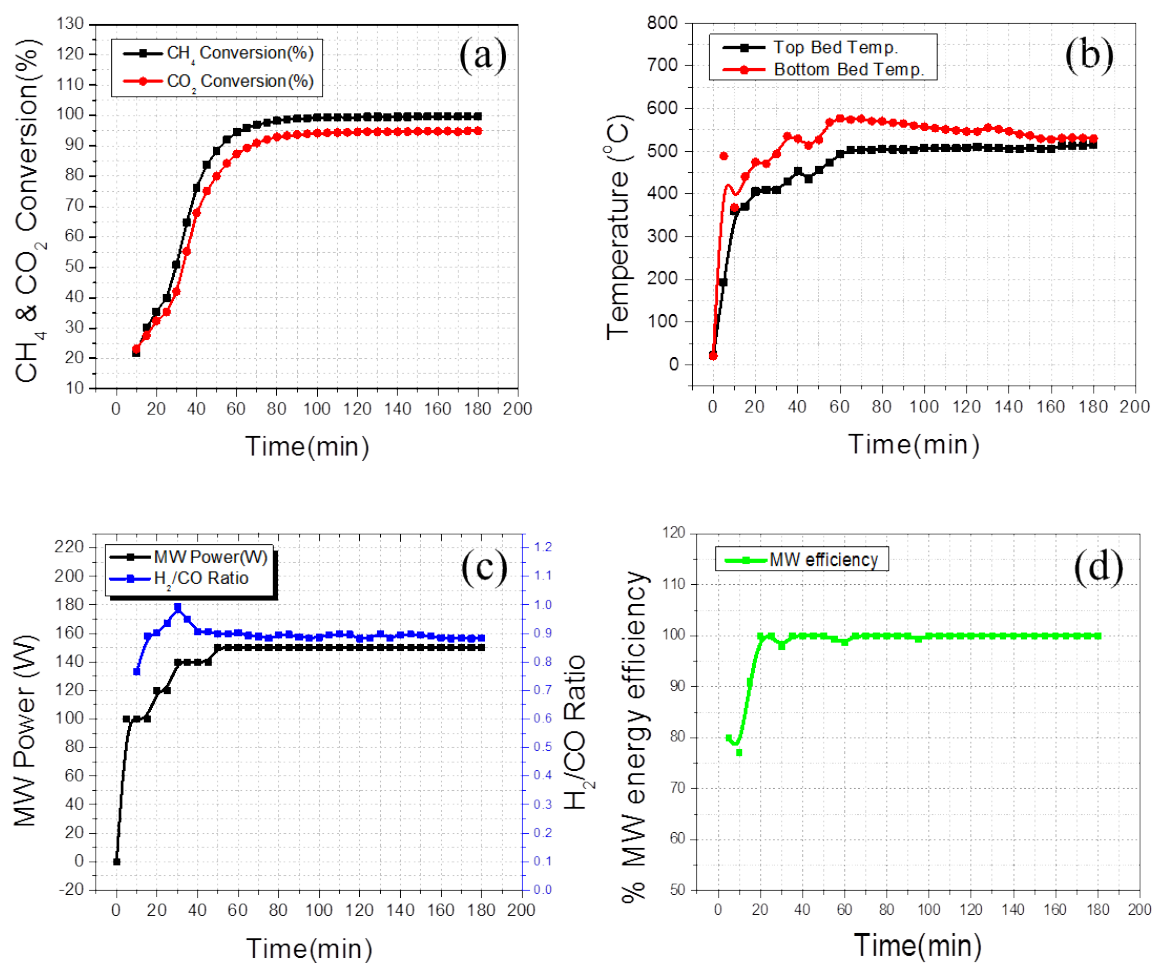

Figure 10. Time-on-stream (TOS) evolution of **(a)** CH_4 and CO_2 conversions, **(b)** top and bottom thermocouple temperature of the catalyst bed, **(c)** MW power and the H_2/CO ratio, and **(d)** % MW energy utilization efficiency during methane dry reforming over the 7Ru/SrTiO₃-MW-1h catalyst. (Reaction conditions: CH_4:CO_2 vol. % feed ratio 45:55, GHSV = 9000 cm³g⁻¹h⁻¹, MW Power: 150 W)

3.3.5 Hotspot detection and temperature gradient analysis

Figure 11 shows the migration of hot spots at (a) 5, (b) 15, (c) 85 and (d) 180 minutes in the $7Ru/SrTiO_3$-MW-1h catalyst bed during the stability test. As thermocouples are placed at the top and bottom part of the catalytic bed, they cannot measure hot spot temperatures inside the catalytic bed. Therefore, we have used the thermocouple and thermal camera dual approach to measure or track the thermal changes occurring in the catalytic bed [19]. Table 4 presents the calculated differences in the hot spot temperatures and the top and average bed temperatures corresponding to the thermal images of Figure 11. All the average bed temperatures and average hot spot temperatures are calculated with a constant emissivity value of 0.8. A more detailed presentation of the thermal camera measurements is given in our recently published article [19].
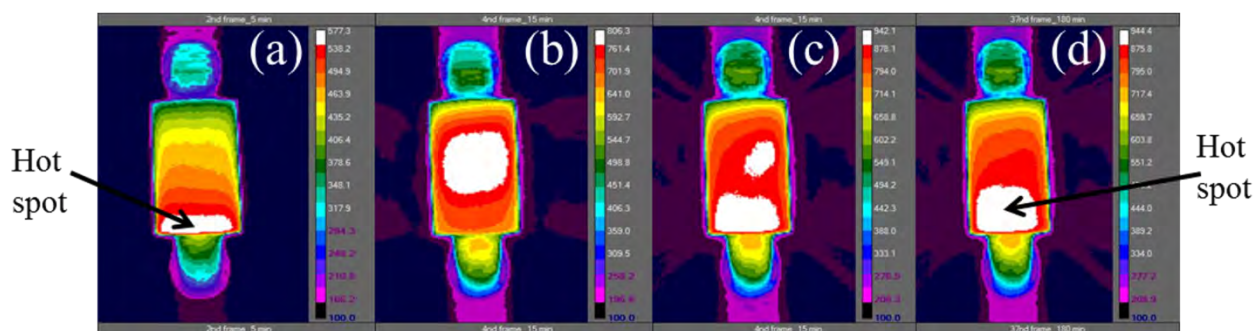

Figure 11. Migration of hot spots during stability test over $7Ru/SrTiO_3$-MW-1h catalyst at **(a)** 5, **(b)** 15, **(c)** 85 and **(d)** 180 minutes. (Reaction conditions: CH_4:CO_2 vol. % feed ratio 45:55, GHSV = 9000 $cm^3g^{-1}h^{-1}$, MW Power: 150 W)

Figure 11a shows that, during the stability test, hotspot generation starts from the bottom part of the catalytic bed (first 5 minutes). At 15 min, the hotspot position is detected at the center of the catalytic bed (Figure 11b) and at 85 minutes, two hotspots are observed, one at the center and one at the bottom part of the catalytic bed (Figure 11c). Finally, at 180 min, one extended hotspot is

observed at the bottom part of the catalytic bed (Figure 11d). The change in the position of the maximum temperature area inside the reactor results in a change in the temperature readings of the top and bottom thermocouples, but, as expected based on Figure 11, the temperature measured by the top thermocouple is always lower than that of the bottom one (Figure 10b).

Table 4: Differences in average hotspot temperature, average catalytic bed temperature, and top and bottom thermocouple temperatures. (Thermal data processed at emissivity 0.8).

Image No	Time (min)	Thermocouple Temperatures(°C)		Average bed temp(°C)	Average hotspot temp (°C)	Average hotspot and average bed temp diff. (°C)	Average hotspot and top thermocouple temp diff. (°C)
		Top T	Bottom T				
(a)	5	192.5	488.5	474.8	579.0	104.25	386.5
(b)	15	370.6	440.4	736.37	813.38	77.01	442.78
(c)	85	504.1	566.6	849.07	936.4	87.38	432.3
(d)	180	514.7	529.7	828.04	942.3	117.3	427.6

As specified in Table 4, the top thermocouple temperatures reported at 5, 15, 85 and 180 min are 192.5, 370.6, 504.1 and 514.7 °C, respectively. The average catalytic bed temperatures calculated by thermal camera analysis are 474.8, 736.37, 849.07 and 828.04 °C. Therefore, it is clear that one-point measurement in case of microwave heating will always provide local temperature values. Hence the comparison of MW heated reactions with conventionally heated reactions using point sensors like thermocouples or optical fibers can be misleading. The temperature difference observed between the average hotspot temperature, and the average catalytic bed temperature is in the range of 77 to 117 °C. The average hotspot and (top) thermocouple temperature difference is in the range of 386.5 to 442.78 °C, which is difficult to trace by point sensors. Therefore, the maximum attained conversions of ~ 99.5% and ~ 94% for CH_4 and CO_2 at ~500 °C, a temperature relatively lower than the required temperature range, are due to the presence of hotspots in the temperature range 813.38 °C to 942.3 °C detected by thermal camera 2D monitoring. The primary reason for hot spot

formation might be the uneven microwave field distribution in the catalytic bed. Santos et al. performed 3D electromagnetic field simulation of a ceramic sample in a microwave oven using COMSOL software and reported that the electromagnetic field pattern changes during MW heating, and so, the hot spots have some type of dynamic behavior [36][37]. The second reason could be the areas where coke formation might have occurred during the MW power variation study. As carbon (coke) is good MW absorber, it might either generate hot spots, or get gasified during the stability test, giving rise to hot spot migration (Fig. 11).

3.3.6 Energy consumption comparison

Table 5 shows a comparison of the newly synthesized perovskite catalyst with carbon-based catalysts reported in the literature for microwave-assisted methane dry reforming [18]. It is shown that H_2 throughput is improved in the case of $7Ru/SrTiO_3$-MW-1h. The amount of catalyst used in the present work has been reduced from 12-15 g to only 1 g in previous studies [18]. The catalytic stability test has been performed at 9000 GHSV as compared to 400 and 3000 GHSV in the case of FY5 (activated carbon) and activated carbon mixed with Ni/Al_2O_3 catalyst, respectively (Table 5). The scale-up energy consumption and H_2 production values based on our experimental results are calculated in a similar way (included as supporting information) as in Fidalgo et al. [18] and compared with the results in [19]. Table 6 presents a comparison on H_2 production and energy consumption in the case of perovskite catalyst and the carbon-based catalysts. Calculations are done on the basis of 1 m^3h^{-1} CH_4 flow rate. The H_2 throughput produced by FY5 is 0.3 $m^3h^{-1}kg^{-1}$ vs. 8.1 $m^3h^{-1}kg^{-1}$ (27 times higher) in the case of $7Ru/SrTiO_3$-MW-1h. The estimated energy consumption is 44.4 kW.h.m^{-3} of H_2 produced for FY5 vs. 18.58 kW.h.m^{-3} of H_2 produced (2.38 times less) for $7Ru/SrTiO_3$-MW-1h.

As regards comparison with the mixed activated carbon and metal-based catalyst (50% FY5 + 50% Ni/Al$_2$O$_3$), Table 6 shows that H$_2$ throughput in the case of 7Ru/SrTiO$_3$-MW-1h is 8.1 m^{3}h^{-1}kg^{-1}, which is ~3.11 times higher than in the case of FY5+NiAl$_2$O$_3$ (2.6 m^3 h^{-1}kg^{-1}). On the other hand, the energy consumption in the case of 7Ru/SrTiO$_3$-MW-1h catalyst is 4 times higher than in the case of FY5+Ni/Al$_2$O$_3$ catalyst (18.58 vs. 4.6 kW.h.m^{-3} of H$_2$ produced, respectively). This may be related to the higher heat losses of the uninsulated reactor in this work that is ~15.7 times smaller than the reported insulated reactor in reference [19]. Finally, the required amounts of FY5, FY5+Ni/Al$_2$O$_3$, and 7Ru/SrTiO$_3$-MW-1h catalysts for the scale-up scenario of 1 m^{3}h^{-1} CH$_4$ flow rate are 6.25, 0.7 and 0.2446 kg, respectively.

Table 5: Catalytic performance comparison of the perovskite catalyst with carbon-based catalysts reported in the literature for microwave-assisted methane dry reforming

Catalyst used	Thermo-couple Temp. (^{o}C)	Feed composition (vol. %)		Amount of catalyst (g)	Flow of CH$_4$ (ml/min)	Total GHSV cm^{3}h^{-1} g^{-1}	Total VHSV Lh^{-1} g^{-1}	MW Power (kW) used at 2.45 GHz	Reactant conversions in %		Reference
		CH$_4$	CO$_2$						CH$_4$	CO$_2$	
FY5 (Activated carbon)	700	40	60	15	40	400	0.4	13.5	96.2	97	[18]
50%FY5 + 50% Ni/Al$_2$O$_3$	800	50	50	12	300	3000	3	11.8	88.1	93.3	[18]
7Ru/SrTiO$_3$-MW-1h	500	45	55	1	67.5	9000	9	0.150	99.5	94	This work.

Table 6: Energy consumption and H$_2$ production comparison of the perovskite catalyst with carbon-based catalysts reported in the literature

Catalyst	FY5 (Activated carbon)	50%FY5 + 50%Ni/Al$_2$O$_3$	7Ru/SrTiO$_3$_ MW_1h	Units
Reference	[18]	[18]	This work	-
Calculation basis	1	1	1	m^3 h^{-1} of CH$_4$
Volume of reactor	912.73	912.73	58.27	cm^3
Amount of catalyst	6.25	0.7	0.2466	kg

Mass inflow rate of CH_4	0.72	0.72	0.72	kg h^{-1}
Mass outflow rate of H_2	0.17	0.16	0.18	kg h^{-1}
Volume outflow rate of H_2	1.92	1.762	1.99	m^3 h^{-1}
Volume outflow rate of H_2 per kg of catalyst	0.3	2.6	8.1	m^3 h^{-1}kg^{-1}
H_2/CO ratio	0.66	1	0.9	-
Supplied power to reactor	84.4	8.3	36.99	kW
Energy consumption w.r.to CH_4 flow	84.4	8.3	36.99	kW.h.m^{-3} of CH_4
Energy consumption w.r.to H_2 flow	44.4	4.6	18.58	kW.h.m^{-3} of H_2

4.   Conclusions

In this work, a series of ruthenium-doped strontium titanate perovskite catalysts were synthesized by conventional and microwave-assisted hydrothermal methods. Significant synthesis temperature and time reduction from 220 °C for 24 h in conventional heating to 180 °C for 1 h under microwave heating were achieved. XRD analysis of the catalyst powder confirmed the presence of Ru in the $SrTiO_3$ perovskite structure in all synthesized catalysts. Increase in the dielectric property values were observed with increase in ruthenium content and temperature. Higher dielectric property values were obtained for the 7 wt. % Ru-doped $SrTiO_3$ catalyst in a tested catalyst series with variable Ru content. Further, ICP-OES analysis and HRTEM+EDX elemental mapping showed improved Ru dispersion and more homogeneous distribution of particle sizes, respectively, in the case of MW-assisted hydrothermal synthesis as compared to the conventional hydrothermal synthesis.

Based on the aforementioned dielectric and chemical characterization study, microwave-assisted methane dry reforming was performed on the 7 wt. % Ru-doped $SrTiO_3$ perovskite catalyst (7Ru/SrTiO$_3$-MW-1h). The influence of different CH_4:CO_2 vol. % feed ratios were studied with respect to their impact on CH_4 conversion. The CH_4:CO_2 vol. % feed ratio 45:55 was found to

maximize methane conversion. Different gas hourly space velocities (GHSVs) of total reactant flows were investigated too. Maximum conversions of ~99.5% and ~94% for CH_4 and CO_2, respectively, were achieved during a 3h stability test at 9000 $cm^3g^{-1}hr^{-1}$ GHSV, with the selected 7 wt. % Ru-doped $SrTiO_3$ catalyst, which was exposed at maximum temperatures in the vicinity of 940 °C. Scale-up calculations on the basis of 1 m^3h^{-1} CH_4 inlet flow rate, as previously set in the literature Ref. [19], on the 7Ru/SrTiO$_3$-MW-1h catalyst show significant improvement in H_2 production capability as compared to carbon-based catalysts.

Acknowledgements

References

[1]   J.M.F. Iii, The Different Catalytic Routes for Methane Liquid Fuels The Different Catalytic Routes for Methane Valorization : An Assessment of Processes for liquid Fuels, 4940 (2016). doi:10.1080/01614949308014605.

[2]   A.I. Olivos-suarez, A. Sze, E.A. Pidko, J. Gascon, Strategies for the Direct Catalytic Valorization of Methane Using Heterogeneous Catalysis : Challenges and Opportunities,

(2016). doi:10.1021/acscatal.6b00428.

[3]   S. Arora, R. Prasad, An overview on dry reforming of methane: strategies to reduce carbonaceous deactivation of catalysts, RSC Adv. 6 (2016) 108668–108688. doi:10.1039/C6RA20450C.

[4]   A. Gvakharia, E.A. Kort, A. Brandt, J. Peischl, T.B. Ryerson, J.P. Schwarz, M.L. Smith, C. Sweeney, Methane, Black Carbon, and Ethane Emissions from Natural Gas Flares in the Bakken Shale, North Dakota, Environ. Sci. Technol. 51 (2017) 5317–5325. doi:10.1021/acs.est.6b05183.

[5]   L. Höglund-Isaksson, Bottom-up simulations of methane and ethane emissions from global oil and gas systems 1980 to 2012, Environ. Res. Lett. 12 (2017) 24007. doi:10.1088/1748-9326/aa583e.

[6]   R. Heede, Tracing anthropogenic carbon dioxide and methane emissions to fossil fuel and cement producers, 1854-2010, Clim. Change. 122 (2014) 229–241. doi:10.1007/s10584-013-0986-y.

[7]   D. Pakhare, J. Spivey, A review of dry (CO2) reforming of methane over noble metal catalysts., Chem. Soc. Rev. (2014). doi:10.1039/c3cs60395d.

[8]   M.C.J. Bradford, M. a. Vannice, CO 2 Reforming of CH 4, Catal. Rev. 41 (1999) 1–42. doi:10.1081/CR-100101948.

[9]   H.R. Gurav, R. Bobade, V.L. Das, S. Chilukuri, Carbon dioxide reforming of methane over ruthenium substituted strontium titanate perovskite catalysts, Indian J. Chem. - Sect. A Inorganic, Phys. Theor. Anal. Chem. 51 (2012) 1339–1347.

[10]   D. Stuerga, P. Gaillard, Microwave heating as a new way to induce localized enhancements of reaction rate. Non-isothermal and heterogeneous kinetics, Tetrahedron. 52 (1996) 5505–5510. doi:10.1016/0040-4020(96)00241-4.

[11]   H.J. Yang, B.P. Mathew, D.G. Oh, K. Myung, J.H. Kwak, S.Y. Hong, Efficient copper catalysts for C[sbnd]H bond arylation under microwave heating: Direct access to multi-substituted pivanilides, Catal. Commun. 90 (2017) 83–86. doi:10.1016/j.catcom.2016.11.022.

[12]   F. Karimi, B.A. Peppley, Comparison of conventional versus microwave heating for polyol synthesis of supported iridium based electrocatalyst for polymer electrolyte membrane water electrolysis, Int. J. Hydrogen Energy. 42 (2017) 5083–5094. doi:10.1016/j.ijhydene.2017.01.090.

[13]   M. Omran, T. Fabritius, R. Mattila, Thermally assisted liberation of high phosphorus oolitic iron ore : A comparison between microwave and conventional furnaces, Powder Technol. 269 (2015) 7–14. doi:10.1016/j.powtec.2014.08.073.

[14]   M. Oghbaei, O. Mirzaee, Microwave versus conventional sintering : A review of fundamentals , advantages and applications, J. Alloys Compd. 494 (2010) 175–189. doi:10.1016/j.jallcom.2010.01.068.

[15]   B. Fidalgo, a. Arenillas, J. a. Menéndez, Influence of porosity and surface groups on the catalytic activity of carbon materials for the microwave-assisted CO2 reforming of CH4, Fuel. 89 (2010) 4002–4007. doi:10.1016/j.fuel.2010.06.015.

[16]   B. Fidalgo, a Dominguez, J. Pis, J. Menendez, Microwave-assisted dry reforming of methane, Int. J. Hydrogen Energy. 33 (2008) 4337–4344. doi:10.1016/j.ijhydene.2008.05.056.

[17]   A. Domínguez, Y. Fernandez, B. Fidalgo, J.J. Pis, J.A. Menendez, Biogas to Syngas by Microwave-Assisted Dry Reforming in the Presence of Char, Energy & Fuels. 21 (2007) 2066–2071. doi:10.1021/ef070101j.

[18]   B. Fidalgo, J. a. Menéndez, Study of energy consumption in a laboratory pilot plant for the microwave-assisted CO2 reforming of CH4, Fuel Process. Technol. 95 (2012) 55–61.

doi:10.1016/j.fuproc.2011.11.012.

[19] L.S. Gangurde, G.S.J. Sturm, T.J. Devadiga, A. Stankiewicz, G.D. Stefanidis, Complexity and challenges in non-contact high temperature measurements in microwave-assisted catalytic reactors, Ind. Eng. Chem. Res. (2017) acs.iecr.7b02091. doi:10.1021/acs.iecr.7b02091.

[20] R.M. Navarro, M.C. Alvarez-Galvan, J.A. Villoria, I.D. González-Jiménez, F. Rosa, J.L.G. Fierro, Effect of Ru on LaCoO3 perovskite-derived catalyst properties tested in oxidative reforming of diesel, Appl. Catal. B Environ. 73 (2007) 247–258. doi:10.1016/j.apcatb.2006.12.013.

[21] J. Sunarso, S.S. Hashim, N. Zhu, W. Zhou, Perovskite oxides applications in high temperature oxygen separation, solid oxide fuel cell and membrane reactor: A review, Prog. Energy Combust. Sci. 61 (2017) 57–77. doi:10.1016/j.pecs.2017.03.003.

[22] D.J. Liu, M. Krumpelt, Activity and structure of perovskites as diesel-reforming catalysts for solid oxide fuel cell, Int. J. Appl. Ceram. Technol. 2 (2005) 301–307. doi:10.1111/j.1744-7402.2005.02032.x.

[23] A. Karaphun, S. Hunpratub, T. Putjuso, E. Swatsitang, Characterization and dielectric properties of SrTi 1− x Mn x O 3 ceramics, Jpn. J. Appl. Phys. 54 (2015) 06FH09. doi:10.7567/JJAP.54.06FH09.

[24] A. Karaphun, S. Hunpratub, E. Swatsitang, Effect of annealing on magnetic properties of Fe-doped SrTiO3 nanopowders prepared by hydrothermal method, Microelectron. Eng. 126 (2014) 42–48. doi:10.1016/j.mee.2014.05.001.

[25] J.M. Catalá-Civera, A.J. Canós, P. Plaza-González, J.D. Gutiérrez, B. García-Baños, F.L. Peñaranda-Foix, Dynamic Measurement of Dielectric Properties of Materials at High Temperature during Microwave Heating in a Dual Mode Cylindrical Cavity, IEEE Trans.

Microw. Theory Tech. 63 (2015) 2905–2914. doi:10.1109/TMTT.2015.2453263.

[26] F.L. Penaranda-Foix, M.D. Janezic, J.M. Catala-Civera, A.J. Canos, Full-wave analysis of dielectric-loaded cylindrical waveguides and cavities using a new four-port ring network, IEEE Trans. Microw. Theory Tech. 60 (2012) 2730–2740. doi:10.1109/TMTT.2012.2206048.

[27] S. Sartipi, S. Xiaohui, T. Cordero, Supporting Information-Carbon / H-ZSM-5 composites as supports for bi-functional Fischer-Tropsch, Catal. Sci. Technol. 5 (2016) 20–23.

[28] R. Cherbański, Calculation of critical efficiency factors of microwave energy conversion into heat, Chem. Eng. Technol. 34 (2011) 2083–2090. doi:10.1002/ceat.201100405.

[29] F. Matei-Rutkovska, G. Postole, C.G. Rotaru, M. Florea, V.I. Pârvulescu, P. Gelin, Synthesis of ceria nanopowders by microwave-assisted hydrothermal method for dry reforming of methane, Int. J. Hydrogen Energy. 41 (2016) 2512–2525. doi:10.1016/j.ijhydene.2015.12.097.

[30] G.S.J. Sturm, M.D. Verweij, T. Van Gerven, A.I. Stankiewicz, G.D. Stefanidis, On the parametric sensitivity of heat generation by resonant microwave fields in process fluids, Int. J. Heat Mass Transf. 57 (2013) 375–388. doi:10.1016/j.ijheatmasstransfer.2012.09.037.

[31] G.S.J. Sturm, M.D. Verweij, A.I. Stankiewicz, G.D. Stefanidis, Microwaves and microreactors: Design challenges and remedies, Chem. Eng. J. 243 (2014) 147–158. doi:10.1016/j.cej.2013.12.088.

[32] M.A. Goula, N.D. Charisiou, G. Siakavelas, L. Tzounis, I. Tsiaoussis, P. Panagiotopoulou, G. Goula, I. V. Yentekakis, Syngas production via the biogas dry reforming reaction over Ni supported on zirconia modified with CeO2 or La2O3 catalysts, Int. J. Hydrogen Energy. 42 (2017) 13724–13740. doi:10.1016/j.ijhydene.2016.11.196.

[33] V. Pawar, D. Ray, C. Subrahmanyam, V.M. Janardhanan, Study of Short-Term Catalyst

Deactivation Due to Carbon Deposition during Biogas Dry Reforming on Supported Ni

Catalyst, Energy and Fuels. 29 (2015) 8047–8052. doi:10.1021/acs.energyfuels.5b01862.

[34] J. a. Menéndez, a. Arenillas, B. Fidalgo, Y. Fernández, L. Zubizarreta, E.G. Calvo, J.M.

Bermúdez, Microwave heating processes involving carbon materials, Fuel Process. Technol.

91 (2010) 1–8. doi:10.1016/j.fuproc.2009.08.021.

[35] X. Zhang, C.S. Lee, D.M.P. Mingos, D.O. Hayward, Carbon dioxide reforming of methane

with Pt catalysts using microwave dielectric heating, 88 (2003) 129–139.

[36] T. Santos, L.C. Costa, M. Valente, J. Monteiro, J. Sousa, 3D Electromagnetic Field

Simulation in Microwave Ovens : a Tool to Control Thermal Runaway, Proc. COMSOL

Conf. (2010) 1–7.

[37] T. Santos, M.A. Valente, J. Monteiro, J. Sousa, L.C. Costa, Electromagnetic and thermal

history during microwave heating, Appl. Therm. Eng. 31 (2011) 3255–3261.

doi:10.1016/j.applthermaleng.2011.06.006.

Supporting Information

Energy Consumption calculations

Table S1: Experimental testing conditions with different units for comparison purpose

Total Flow rate	150 ml/min	9 Lh-1	9000 cm³h⁻¹
CH₄ Flow rate	67.5 ml/min	4.05 Lh-1	4050 cm³h⁻¹
CO₂ Flowrate	82.5 ml/min	4.95 Lh-1	4950 cm³h⁻¹
Weight of Catalyst used	1 g	0.001 kg	0.001 kg
MW Power Supplied	150 W	0.150 kW	0.150 kW
GHSV	-	9 Lg-1h-1	9000 cm³g⁻¹h⁻¹
CH₄:CO₂ Volume % ratio used	-	-	45:55
CH₄ conversion	-	-	99.5 %
CO₂ conversion	-	-	94%

Volume of quartz reactor used in reference [19]

$$Volume\ of\ quartz\ tube = \pi * (Diameter)^2 * Length = \pi * (2.6\ cm)^2 * 43\ cm = \mathbf{912.73\ cm^3}$$

Volume of quartz reactor used in our work

$$Volume\ of\ quartz\ tube = \pi * (Diameter)^2 * Length = \pi * (0.8\ cm)^2 * 29\ cm = \mathbf{58.27\ cm^3}$$

Scale up calculations

For 1 m³h⁻¹ of CH_4 reforming:

To perform the reforming of 1 m³h⁻¹ of CH_4 inlet flow rate at 9 Lg⁻¹h⁻¹ VHSV space velocity, the required amount of catalyst is calculated as follows

Note: we need to consider 45:55 volume % of CH_4: CO_2 ratio. Therefore, the total flow rate of the reactants becomes 2.22 m³h⁻¹.

$$VHSV = \frac{Total\ flow(m^3h^{-1})}{Amount\ of\ catalyst(kg)} = 9\ Lh^{-1}g^{-1} = \frac{2.22\ m^3h^{-1}}{Amount\ of\ catalyst(kg)}$$

$$Amount\ of\ catalyst = \frac{2.22\ m^3h^{-1}}{9\ Lh^{-1}g^{-1}} = 0.2466\ kg$$

Therefore, 0.2466 kg of 7Ru/SrTiO3-MW-1h catalyst will be needed to process a total flow rate of 2.22 m^3h^{-1} of 45%CH_4-55%CO_2.

We used 150 W of MW power for 1 g of catalyst at 9 $Lh^{-1}g^{-1}$ GHSV. The power needed to keep the reaction system running at 2.22 m³h⁻¹ total flow is calculated as

$$\text{Specific Power} = \frac{Power\ required\ for\ 2.22\ m^3h^{-1}}{Amount\ of\ Catalyst\ used}$$

Therefore if we assume our specific power is 150 kWkg⁻¹.

$$150\ (\text{kWk}g^{-1}) = \frac{Power\ Required(kW)}{0.2466\ kg}$$

Then, the power required for 1m³h⁻¹ CH_4 conversion is 36.99 kW.

The hydrogen flowrate based on 1 m³ hr⁻¹ CH_4 flowrate and experimentally obtained CH_4 conversion is calculated as

$$\text{Flow rate of hydrogen} = \text{inlet } CH_4 \text{ flow rate} * \%\ CH_4\ \text{Conversion} * 2$$

Flow rate of hydrogen $= 1$ m³hr⁻¹*0.995*2 $= 1.99$ m³hr⁻¹

Energy Consumption w.r.t 1 m³ hr⁻¹ CH_4 flow keeping VHSV constant

$$\text{Energy Consumption w.r.t } CH_4 \text{ flow} = \frac{Power\ required(kW)}{Flowrate\ of\ methane(m^3h^{-1})} = \frac{36.99}{1} = 36.99\ \text{kW.h.m}^{-3}$$

Energy Consumption w.r.t H_2 flow keeping VHSV constant

$$\text{Energy Consumption w.r.t. } H_2 \text{ flow} = \frac{Power\ Required(kW)}{Flowrate\ of\ Hydrogen(m^3h^{-1})} = \frac{36.99}{1.99} = 18.58\ \text{kW.h.m}^{-3}$$

Density of CH_4 at NTP is 0.668 and at STP is 0.717 kg/m³

Density of H_2 at NTP is 0.0899 and at STP is 0.0899 kg/m³

Therefore, the inlet flow rate of CH_4 in terms of kgh⁻¹ is calculated by its density

$$\text{Density} = \frac{Mass(kg)}{Volume\ (m^3)} = 0.717 = \frac{Mass(kg)}{1\ (m^3)}$$

Therefore, the mass flow rate of CH_4 is 0.72 kg/h.

The mass flow rate of hydrogen produced is calculated from

$$0.0899 = \frac{Mass(kg)}{1.99(m^3)}$$

So, H_2 is produced at 0.18 kg/h.

The amount of H_2 produced per kg of catalyst is calculated from

$$H_2 \text{ Produced per kg cat.} = \frac{\text{Outlet } H_2 \text{ flow in } m^3h^{-1}}{\text{Amount of catalyst in kg}} = \frac{1.99 \text{ } m^3h^{-1}}{0.2466 \text{ kg cat.}} = 8.1 \text{ } m^3h^{-1}kg^{-1}$$